A reversal in global terrestrial stilling and its implications for wind energy production

Zhenzhong Zeng [1,2]*, Alan D. Ziegler [3], Timothy Searchinger[4], Long Yang [5], Anping Chen [6], Kunlu Ju [7], Shilong Piao [8], Laurent Z. X. Li [9], Philippe Ciais [10], Deliang Chen [11], Junguo Liu [1], Cesar Azorin-Molina [11,12], Adrian Chappell [13], David Medvigy [14] and Eric F. Wood [2]

Wind power, a rapidly growing alternative energy source, has been threatened by reductions in global average surface wind speed, which have been occurring over land since the 1980s, a phenomenon known as global terrestrial stilling. Here, we use wind data from in situ stations worldwide to show that the stilling reversed around 2010 and that global wind speeds over land have recovered. We illustrate that decadal-scale variations of near-surface wind are probably determined by internal decadal ocean–atmosphere oscillations, rather than by vegetation growth and/or urbanization as hypothesized previously. The strengthening has increased potential wind energy by $17 \pm 2\%$ for 2010 to 2017, boosting the US wind power capacity factor by ~2.5% and explains half the increase in the US wind capacity factor since 2010. In the longer term, the use of ocean–atmosphere oscillations to anticipate future wind speeds could allow optimization of turbines for expected speeds during their productive life spans.

R eports of a global decline in land surface wind speed of 8% from ~1980 to 2010 have raised concerns about outputs from future wind power[1–5]. Wind power (p) varies with the cube of wind speed (u) according to the formula:

$$p = \frac{\rho s f}{2} u^3 \tag{1}$$

where ρ is air density, s is the swept area of the turbine and f is an efficiency factor[6]. The decline has been manifested in the northern mid-latitude countries where the majority of wind turbines are installed, including China, the United States and Europe[1]. If the observed trend from 1980 to 2010 were to continue to the end of the century, global wind speed would reduce by 21%, halving the amount of power available in the wind (using equation (1)). Understanding the drivers of this long-term decline in wind speed is critical, not only to maximize wind energy production[7–9] but also to address other globally significant environmental problems related to terrestrial stilling, including reduced aerosol dispersal, changes in evapotranspiration rates and adverse effects on animal behaviour and ecosystem functioning[1,3,4,10].

The potential causes for the global terrestrial stilling are complex and remain contested[2,3,11,12]. Many regional-scale studies[13–17] using reanalysis datasets have found correlations of wind speed with various climate indices. Those studies hypothesize that terrestrial stilling is caused by changes in large-scale circulations[11], which manifest as consistent wind speed changes at the surface and at higher levels in reanalysis datasets[11,14]. Nevertheless, there are large uncertainties in

these datasets[2,11,14] and, more importantly, global terrestrial stilling is either not reproduced or it has been largely underestimated in global reanalysis products[2,11] (Supplementary Fig. 1) and/or climate model simulations for the IPCC Fifth Assessment Report[8] (Supplementary Fig. 2). Acknowledging that wind speed reanalysis datasets do not represent land surface dynamics, the discrepancies between the decreasing trends derived from in situ stations and from reanalysis or climate model simulations lead to the hypothesis that global terrestrial stilling is caused by increased drag related to increased surface roughness from the greening of the Earth and/or urbanization[2,18], both of which would suggest further declines in the future.

However, conversely, recent studies have described wind speed reversal at local scales[19,20] or an increase of global wind speed during a particular year[21], despite uncertainty over the global trend of wind speed change[5,11]. The recent reversal over land, if evidenced to be true at the global scale, could elucidate the causes of global terrestrial stilling and potentially improve future wind energy projections.

Analysis

We integrate direct in situ observations of wind speed from ground weather stations from 1978 to 2017 with statistical models for detection of trends. The stations, mainly distributed in the northern mid-latitude countries, were carefully selected from the Global Summary of Day (GSOD) database following strict quality control procedures (Supplementary Fig. 3; see Methods for details). To test for a continuation of the terrestrial stilling after 2010 (refs. [1–4]), we use a piecewise linear regression model to examine the potential trend changes[22,23].

[1]School of Environmental Science and Engineering, Southern University of Science and Technology, Shenzhen, China. [2]Department of Civil and Environmental Engineering, Princeton University, Princeton, NJ, USA. [3]Geography Department, National University of Singapore, Singapore, Singapore. [4]Woodrow Wilson School, Princeton University, Princeton, NJ, USA. [5]School of geography and ocean science, Nanjing University, Nanjing, China. [6]Department of Biology, Colorado State University, Fort Collins, CO, USA. [7]School of Economics and Management, Tsinghua University, Beijing, China. [8]Sino-French Institute for Earth System Science, College of Urban and Environmental Sciences, Peking University, Beijing, China. [9]Laboratoire de Météorologie Dynamique, Centre National de la Recherche Scientifique, Sorbonne Université, Ecole Normale Supérieure, Ecole Polytechnique, Paris, France. [10]Laboratoire des Sciences du Climat et de l'Environnement, CEA CNRS UPSACLAY, Gif-sur-Yvette, France. [11]Regional Climate Group, Department of Earth Sciences, University of Gothenburg, Gothenburg, Sweden. [12]Centro de Investigaciones sobre Desertificación, Consejo Superior de Investigaciones Científicas, Montcada, Valencia, Spain. [13]School of Earth and Ocean Sciences, Cardiff University, Cardiff, UK. [14]Department of Biological Sciences, University of Notre Dame, Notre Dame, IN, USA. *e-mail: zzeng@princeton.edu
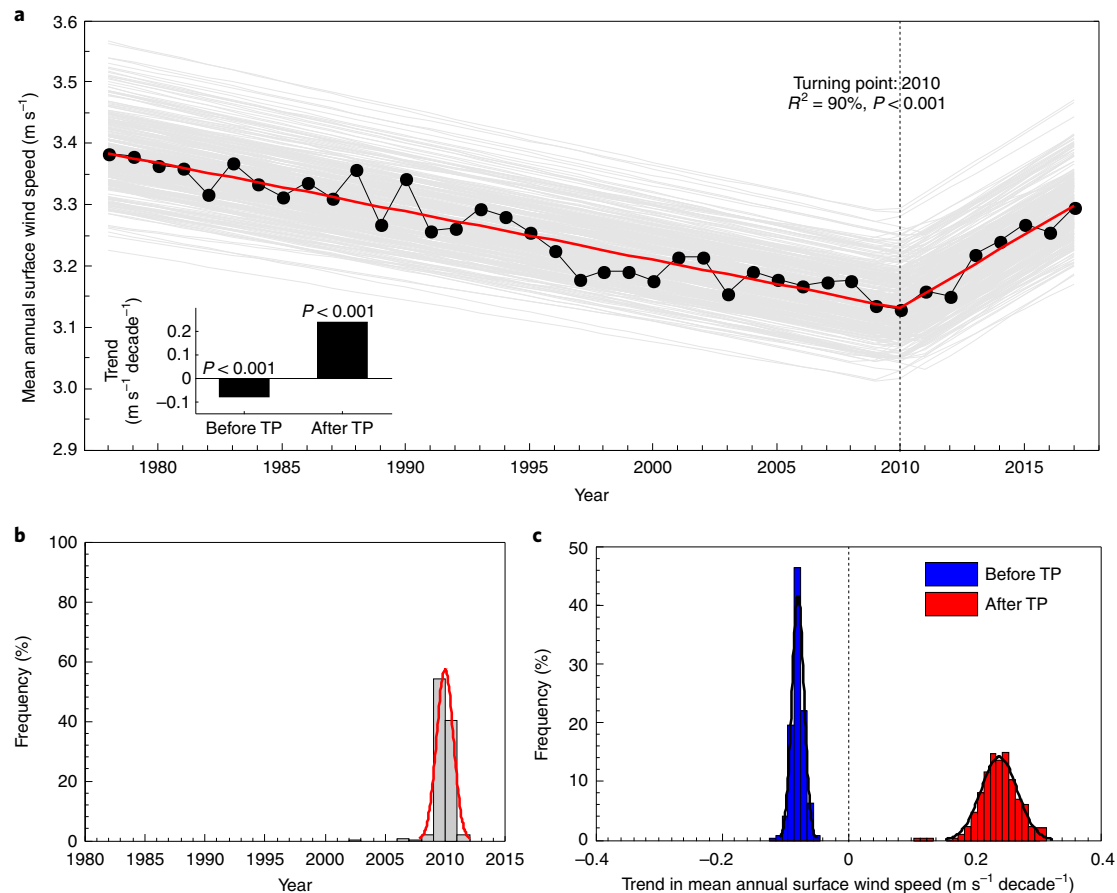
Fig. 1 | Turning point for mean global surface wind speed. a, Global mean annual wind speed during 1978–2017 (black dots and line). The piecewise linear regression model indicates a statistically significant turning point (TP) in 2010. The red line is the piecewise linear fit ($R^2 = 90\%$, $P < 0.001$). The dashed line indicates the turning point. The trends before and after the turning point are shown in the inset. Each grey line ($n = 300$) is a piecewise linear fit for a randomly selected subset (40%) of the global stations. **b**, Frequency distribution of the estimated turning points derived from 300 resampling results. **c**, Frequency distribution of the trends in mean annual wind speed before and after the turning points identified in the 300 resampling results. The result is based on the weather stations in the GSOD database.

Scope of a reversal in global terrestrial stilling

The analysis shows that global mean annual wind speed decreased significantly at a rate of -0.08 m s^{-1} decade^{-1} (or -2.3%) during the first three decades, beginning from 1978 ($P < 0.001$; Fig. 1a, Supplementary Table 1). Although the decreasing trend has previously been shown[2–4] and confirms global terrestrial stilling as an established phenomenon during the period of 1978–2010, we find that wind speed has significantly increased in the current decade. This turning point is statistically significant at $P < 0.001$, with a goodness-of-fit of $R^2 = 90\%$ (Fig. 1a). The recent increasing rate of 0.24 m s^{-1} decade^{-1} ($P < 0.001$) is threefold the decreasing rate before the turning point in 2010.

To exclude the possibility that the turning point is caused by large wind speed changes at only a few sites, we repeat our analyses 300 times by randomly resampling 40% of the global stations each time (grey lines in Fig. 1a; 40% of the stations are selected to ensure a sufficient sample size ($n > 500$)). We find significant turning points in each randomly selected subsample ($P < 0.001$; $R^2 \geq 76\%$). Run-specific turning points occur between 2002 and 2011, with most (95%) of them between 2009 and 2011 (Fig. 1b). In addition, mean annual wind speed changes before and after a specific turning point based on the 300 subsample estimates are -0.08 ± 0.01 m s^{-1} decade^{-1} and 0.24 ± 0.03 m s^{-1} decade^{-1}, respectively (Fig. 1c), which are identical to those values based on all global samples.

Spatial analyses further confirm that the recent reversal is a global-scale phenomenon (Supplementary Fig. 4a–c). A majority (79%) of the stations where wind speed decreased significantly during 1978–2010 (Supplementary Fig. 4b) have positive trends after 2010 (Supplementary Fig. 4c). The stations are mainly distributed over North America, Europe and Asia. Significant turning points exist in all three regional mean annual wind speed time series ($P < 0.001$, Supplementary Fig. 4d–f), but they vary in the specific year of occurrence. For example, a turning point occurs earlier in Asia (2001, $R^2 = 80\%$, Supplementary Fig. 4f) and Europe (2003, $R^2 = 56\%$, Supplementary Fig. 4e) than in North America (2012, $R^2 = 80\%$, Supplementary Fig. 4d). Nevertheless, all three regions have the most significant increase in wind speed after ~2010 (Supplementary Fig. 4d–f).

The existence of turning points is robust, regardless of season (Supplementary Table 1 and Fig. 5) or wind variable chosen for analysis (Supplementary Fig. 6), and shows no dependence on quality control procedures for weather station data (Supplementary Fig. 7). For maximum sustained wind and wind gusts, the turning points appear earlier and the recent increasing rates are weaker (Supplementary Fig. 6). Furthermore, we show that our findings are robust and repeatable (Supplementary Fig. 8) using a different dataset—the HadISD database, which follows station selection criteria and a suite of quality control tests established by the UK

Met Office Hadley Centre[24]. We also find that the tendency for an increasing number of stations becoming automated during recent decades (Supplementary Figs. 9 and 10) does not affect the result (Supplementary Fig. 11). Finally, to test the effect of inhomogeneity, we remove all the stations with change points detected by Pettitt tests[25]. After removal, the results do not change when the analysis is repeated (Supplementary Fig. 12). All these lines of evidence provide independent support that the trends in wind speed are not caused by changes in measurement methods and inhomogeneity.

Causes of the reversal in global terrestrial stilling

A variety of theories have been presented previously to explain stilling, many of which focus on the drag force of wind speed linked to increased terrestrial roughness caused by urbanization and/or vegetation changes[2,12]. These theories are contested[26] (see Supplementary Figs. 13 and 14). Our finding of a global stilling change after 2010, and especially the finding of an increasing rate that is three times of the decreasing rate before 2010 (Fig. 1a), are counter to these theories. Terrestrial roughness did not suddenly change in 2010. More likely, the variation in wind speed (including prior stilling and the recent reversal) is determined mainly by driving forces associated with decadal variability of large-scale ocean–atmospheric circulations.

Wind is created by pressure gradients associated with uneven heating of the Earth's surface (temperature anomalies or heterogeneity), and heterogeneity is to a large extent described by climate indices for oscillations. To test such associations, we first include 21 climate indices in the pool of indicators for ocean–atmosphere oscillations (Supplementary Table 2 and Methods). To avoid overfitting, we apply stepwise regression[27] to identify the six largest explanatory power factors for the decadal variations of wind speed over the globe, North America, Europe and Asia (see Supplementary Table 3). The reconstructed wind speed obtained from the stepwise linear regression matches well with the observed wind speed (Supplementary Figs. 15 and 16, and discussion in Methods). Finally, we train our models using only the detrended time series before the turning points (2010 for the globe, 2012 for North America, 2003 for Europe and 2001 for Asia), finding that the models are capable of reproducing the positive trends after the turning points, not only for the globe ($P < 0.001$; Fig. 2a), but also for all three regions ($P < 0.001$; Fig. 2b–d). The magnitude of the increasing rate after the turning points is well modelled (Fig. 2). These results suggest a predictive relationship between wind changes and ocean–atmosphere oscillations, which would be valuable for the wind energy sector.

We further construct the composite annual mean surface temperature for the years that exhibit negative (Fig. 3a) and positive (Fig. 3b) anomalies of detrended wind speed. During the years of negative wind speed anomalies (Fig. 3a) the following are observed: (1) positive anomalies of temperature prevail over the tropical northern Atlantic (5.5° N to 23.5° N, 15° W to 57.5° W), showing a positive value for the Tropical Northern Atlantic Index (TNA); (2) the west (east) Pacific is warmer (colder) than that in normal years, demonstrating a negative value for the Pacific Decadal Oscillation (PDO) and (3) positive anomalies of temperature occur near the Azores and negative anomalies occur over Greenland, indicating a negative value for the North Atlantic Oscillation (NAO). The opposite pattern (that is, negative TNA and positive PDO and NAO) occurs during the years of positive wind speed anomalies (Fig. 3b). Furthermore, TNA has strong, significant and negative correlations with regional wind speed, particularly over North America (Fig. 3c); PDO has significant positive correlations with regional wind speed globally (Fig. 3e) and NAO has overwhelmingly significant positive correlations with regional wind speed in the United States and Northern Europe, but negative correlations with regional wind speed in Southern Europe (Fig. 3d). These patterns are consistent with the finding that the greatest explanatory power factor is TNA for North America ($R = -0.67$, $P < 0.001$), PDO for Asia ($R = 0.50$,

$P < 0.01$) and NAO for Europe ($R = 0.37$, $P < 0.05$) (for more discussion refer to Methods). The ocean–atmosphere oscillations, characterized as the decadal variations in these climate indices (mainly TNA, NAO, PDO), can therefore explain the decadal variation in wind speed (that is, the long-term stilling and the recent reversal) (Figs. 2 and 3f–h).

Several theories[28–31] have tried to identify potential physical mechanisms describing how various ocean–atmosphere oscillations affect regional wind speed over land. With respect to TNA, prior studies demonstrate that the positive phase of TNA is linked with a weakened Hadley circulation (for details of the theory refer to ref. [28]). We also find that during the positive phase of TNA a cold anomaly occurs over the eastern coast of the United States (Fig. 3a and ref. [28]). This pattern leads to a southward component of surface wind and a stable environment of weak convergence from the tropics to the mid-latitudes, resulting in a reduction of wind speed in the mid-latitudes and particularly in the United States (Fig. 3c and Supplementary Fig. 17a,b). As for NAO, its negative and positive phases have different jet stream configurations and wind systems in northern versus southern Europe (Supplementary Fig. 17c,d and refer to ref. [29]). During the positive (negative) phase, the pressure gradient across the North Atlantic[29] generates strong winds and storms across northern (southern) Europe (Supplementary Fig. 17c,d), explaining the contrasting correlations of NAO to wind speed in these two regions (Fig. 3d and Supplementary Fig. 18). For PDO, the temperature gradient during the negative (positive) phase generates an easterly (westerly) component of surface wind (refer to refs. [30,31]), which weakens (strengthens) the prevailing westerly winds in the mid-latitudes (Supplementary Fig. 17e,f) and explains the widespread and significant positive correlations between PDO and wind speed across the whole mid-latitudes (Fig. 3e). Despite these potential physical mechanisms[28–31], the relationships between ocean–atmosphere oscillations and long-term wind speeds over land are still uncertain and require more investigation.

Finally, it is critical to determine why global reanalysis products do not reproduce or underestimate the historical terrestrial stilling (Supplementary Fig. 1), which is a major basis for prior studies[2,12] rejecting ocean–atmosphere oscillations as a dominant driver for terrestrial stilling. Although global reanalysis products are generated at numerical weather prediction centres with advanced data assimilation systems, most cannot assimilate near-surface winds over land satisfactorily due to inappropriate model topography and inaccuracy of atmospheric boundary layer processes that are implemented into the data assimilation systems. ERA-Interim[32], one of the best products available, can only assimilate surface winds over seas from scatterometers, ships and buoys. The capacities of these products in reproducing the near-surface wind speed over land are thus generally poor and rely on climate models. We find that in the regions where Atmospheric Model Intercomparison Project model simulations (that is, atmospheric simulations forced with observed sea surface temperature (SST)) capture the stilling, such as Europe and India (fig. 4a,b in ref. [26]), the global reanalysis products are also capable of reproducing the stilling (Supplementary Fig. 1c). In contrast, for regions where Atmospheric Model Intercomparison Project simulations do not capture the stilling, such as North America[26,33], the global reanalysis products fail to reproduce the stilling[2,11] (Supplementary Fig. 1b). Model limitations are therefore probably the reason preventing global reanalysis products from reproducing the observed near-surface wind speed changes in some regions. More efforts are required to improve surface process parameterization schemes and their connections to ocean–atmosphere circulations in climate models and operational weather data assimilation systems.

Implications for wind energy production

In wind power assessments, near-surface wind observations from weather stations (u at height $z_s = 10$ m) are often used to estimate
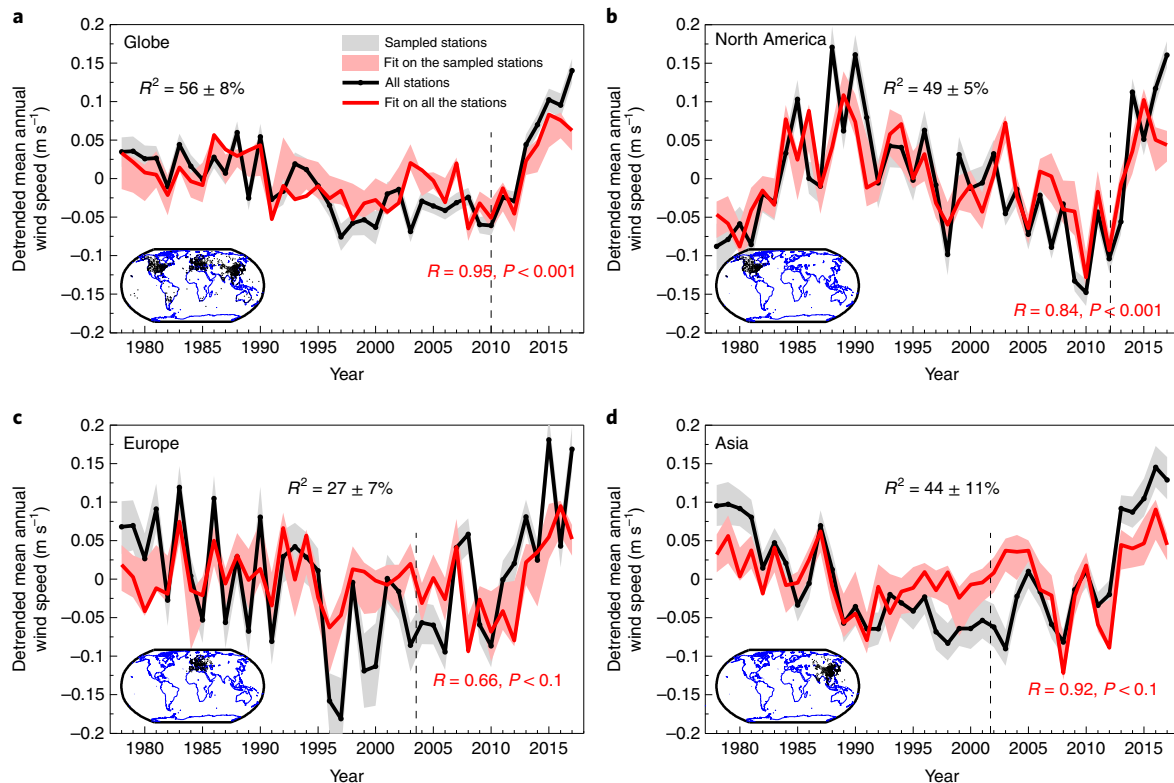
Fig. 2 | The decadal variations in wind speed can be reconstructed by ocean/atmosphere oscillations. a–d, Observed (black) and reconstructed (red) detrended mean annual wind speed over the globe (**a**), North America (**b**), Europe (**c**) and Asia (**d**). The dashed line indicates the turning point (2010 for the globe, 2012 for North America, 2003 for Europe and 2001 for Asia). For the globe and each of the three continents, we select the six largest explanatory climate indices for the decadal variations of wind speed with a stepwise forwarding regression model, using only the detrended time series before the turning points. The selected climate indices are then used to reconstruct decadal variations of wind speed via a multiple regression. Uncertainties are the interquartile range of the results based on a randomly selected 40% subset of the station pools (repeated 300 times). Inset plots indicate the locations of the stations. Inset black numbers are coefficients of determination between observed and reconstructed wind speed before the turning points. Inset red numbers are correlation coefficients and their significance between observed and reconstructed wind speed after the turning points.

wind speeds at the height of a turbine (u_{tb} at height $z_{tb} = 50$–150 m) using an exponential wind profile power law relationship:

$$u_{tb} = u \left(\frac{z_{tb}}{z_s} \right)^{\alpha} \tag{2}$$

where α is commonly assumed to be constant (1/7) in wind resource assessments because the differences between these two levels are unlikely to be great enough to introduce considerable errors in the estimates[5].

Changes in wind speed matter not only on average but also in the percentage of the time that the wind speeds are high or low. A velocity of $u_{tb} > 3$ m s^{-1} is a typical minimum value needed to drive turbines efficiently and therefore, wind speeds below 3 m s^{-1} are typically wasted from the power generation perspective. Although periods of high wind speed greatly increase the physical capacity to generate power according to equation (1), turbines are built with a maximum capacity, and so periods of high wind speed can also 'waste' the uses of wind with the threshold depending on the capacity of the turbine.

On average, the rise of global mean annual wind speed from 3.13 m s^{-1} in 2010 to 3.30 m s^{-1} in 2017 (Fig. 1a; see Methods for details) increases the amount of energy entering a hypothetical wind turbine receiving the global average wind by $17 \pm 2\%$ (uncertainty is associated with subsamples in Fig. 1a; regionally, $22 \pm 2\%$ for North America, $22 \pm 4\%$ for Europe and $11 \pm 4\%$ for Asia). At the hourly scale, the frequency of low wind speed decreases

while the frequency of high wind speed increases (Fig. 4a). Using a General Electric GE 2.5-120 turbine[34] (Supplementary Fig. 19) for illustration, the effects of changes in global average wind speed increase potential power generation from 2.4×10^6 kWh in 2010 to 2.8×10^6 kWh in 2017 (+17%). If the present trend persists for at least another decade, in light of the robust increasing rate during 2010–2017 (Fig. 1a) and the long cycles of natural ocean–atmosphere oscillations[28–31,35] (Supplementary Fig. 20), power would rise to 3.3×10^6 kWh in 2024 (+37%), resulting in a +3% decade^{-1} increase of global average capacity factor (mean power generated divided by rated peak power). This change is even larger than the projected change in wind power potential caused by climate change under multiscenarios[36].

During the past decade, the capacity factor of the US wind fleet[37] has steadily risen at a rate of +7% decade^{-1} (Fig. 4b) and it was previously attributed only to technology innovations[38]. We find that the capacity factor for wind generation in the United States is highly and significantly correlated with the variation in the cube of regional-average wind speed (u^3, $R = 0.86$, $P < 0.01$; Fig. 4b). To isolate the wind speed-induced increase in capacity factor from that due to technology innovations, we use the regional mean hourly wind speed in 2010 and 2017 to estimate the increase of capacity factor for a given turbine, thereby controlling for technology innovations. It turns out that the increased cube of the regional-average wind speed explains ~50% of the increase of the capacity factor (see Methods for details). Therefore, in addition to technology innovations, the strengthening wind speed is another key factor
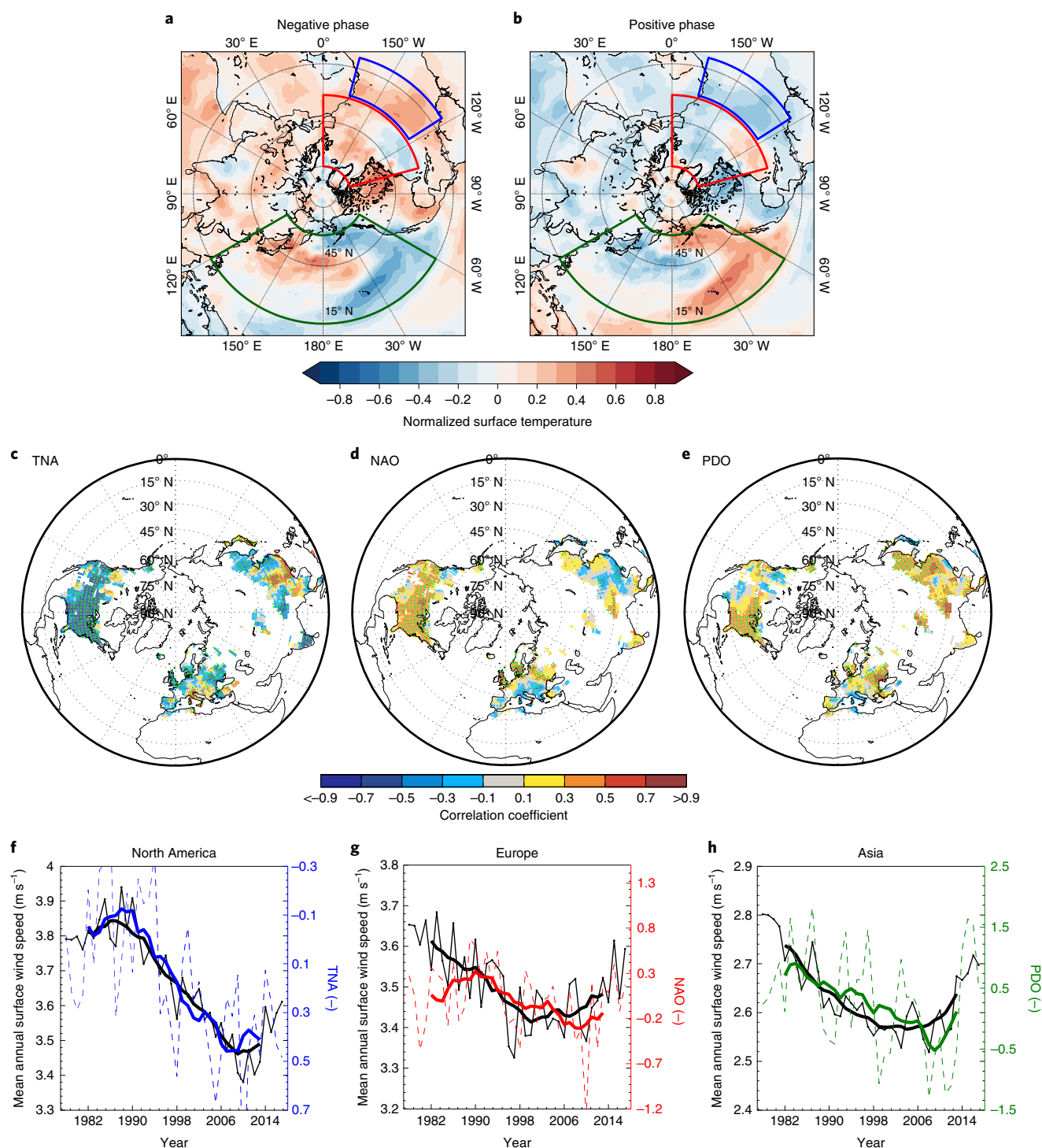
Fig. 3 | Mechanisms for the decadal variation in wind speed. a,b, Normalized mean annual surface temperature for the years with negative (**a**) and positive (**b**) anomalies of detrended wind. Characteristic regions for PDO, NAO and TNA are outlined by green, red and blue polygons, respectively. Surface temperature over land is obtained from Climate Research Unit TEM4 with a spatial resolution of 5° × 5° (ref. [42]) and over ocean from NOAA Optimum Interpolation Sea Surface Temperature V2, with a spatial resolution of 1° × 1° (ref. [43]). **c–e**, Spatial patterns of the correlation between the regional (5° × 5°) mean annual wind speed and TNA (**c**), NAO (**d**) and PDO (**e**) for 1978–2017. The green dots represent significance at *P* < 0.05 level. **f–h**, Decadal variations are shown for TNA and regional wind speed in North America (**f**), NAO and regional wind speed in Europe (**g**) and PDO and regional wind speed in Asia (**h**). The thin lines are annual values and the thick lines are 9-yr-window moving averages. The black lines are wind speed and the coloured lines are TNA (blue), NAO (red) and PDO (green).

powering the increasing efficiency of wind power production in the United States (and other mid-latitude countries where wind speed is increasing, such as China and European countries).

One turbine (General Electric GE 1.85-87 (ref. [39])) installed at one of our in situ weather stations in the United States in 2014 (inset plot in Fig. 4c) is selected to illustrate the consequences. The
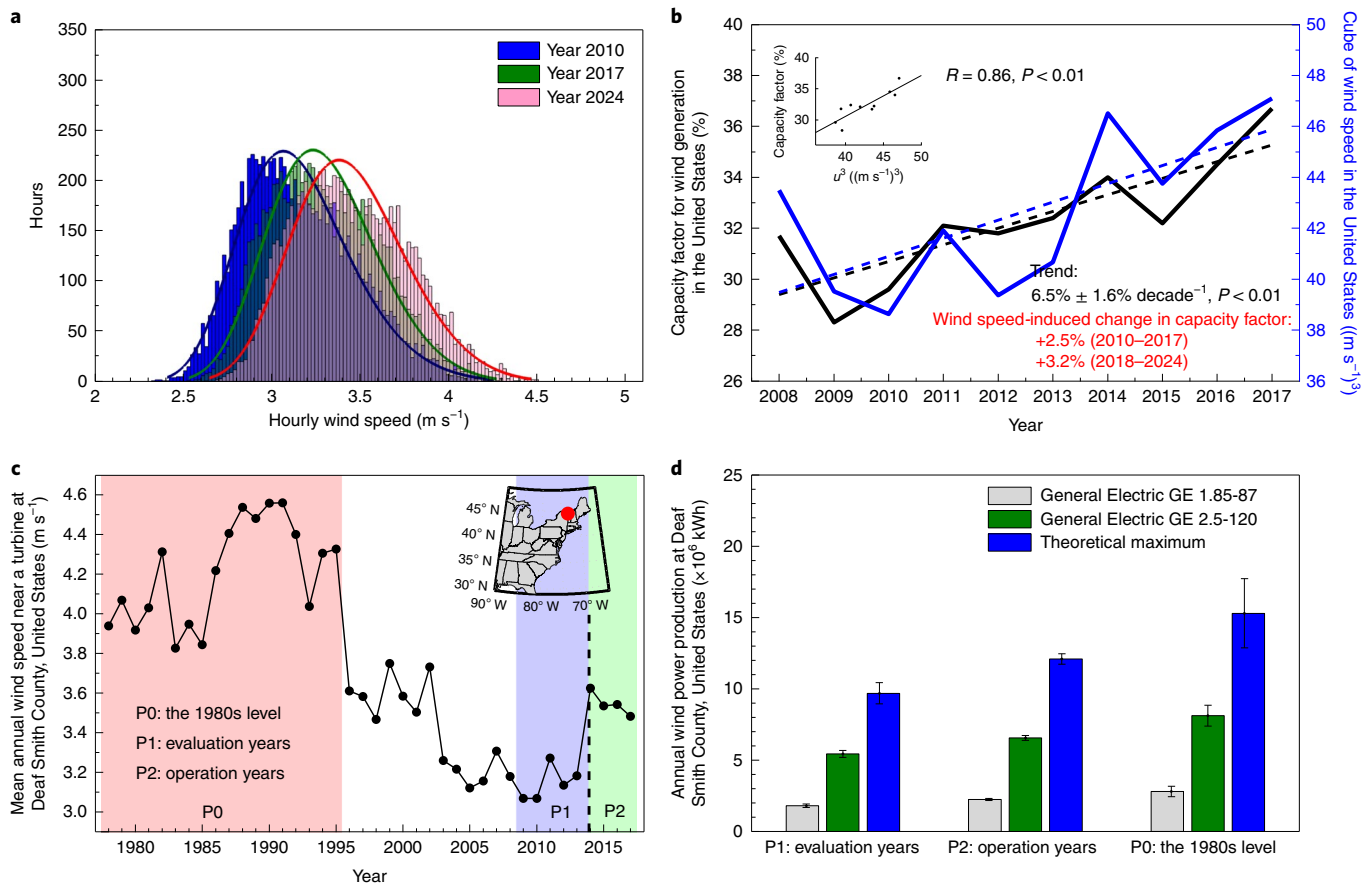
Fig. 4 | Implications of the recent reversal in global terrestrial stilling for the wind energy industry. a, Frequency distribution of global mean hourly wind speed in 2010 and 2017, and the year 2024 assuming the same increasing rate as that during 2010–2017. The density curves from the respective generalized extreme value distributions are also provided (lines). **b**, Time series of the overall capacity factor for wind generation in the United States (black line) and the cube of the regional-average wind speed (blue line) from 2008 to 2017. The inset scatter plot shows the significant relationship between the overall capacity factor and the cube of the regional-average wind speed ($R = 0.86$, $P < 0.01$). The inset black numbers show the trend in the overall capacity factor for wind generation, and the inset red numbers show the wind speed-induced increase of capacity factor in the United States. **c**, Mean annual wind speed observed at a weather station near an installed turbine at Deaf Smith County in the United States (<1 km; location shown in the inset). The turbine was installed in 2014. The background colours separate different periods: P0, the 1980s level when wind speed is relatively strong (1978–1995); P1, the evaluation years before the installation of the turbine (2009–2013) and P2, the operation years when the turbine was generating power (2014–2017). **d**, Mean annual wind power production at Deaf Smith County from different wind turbines during the three periods of reference (grey: General Electric GE 1.85-87; green: General Electric GE 2.5-120 turbine; blue: the theoretical maximum of power that can be extracted by a wind turbine with a diameter of 120 m and hub height of 120 m constrained by the Betz limit). Error bars show the interannual variability within the periods.

turbine was expected to produce $1.8 \pm 0.1 \times 10^6$ kWh using four years of wind speed records before the installation (2009–2013)[39], but actually produced $2.2 \pm 0.1 \times 10^6$ kWh between 2014 and 2017 (+25%). This system has the potential to generate $2.8 \pm 0.1 \times 10^6$ kWh (+56%) if wind speed recovers to the 1980s level (red bars in Fig. 4d; see Methods for details). Globally, 90% of the cumulative wind capacity has been installed in the last decade[40], during which the global-average wind speed has been increasing (see above).

Discussion

Although the response of ocean–atmosphere oscillations to anthropogenic warming remains unclear[31], the increases in wind speeds should continue for at least a decade because these oscillations change over decadal time frames[28–31,35]. Climate model simulations constrained with historical SST also show a long cycle in wind speed over land (Supplementary Fig. 20). Our findings are therefore good news for the power industry for the near future.

However, oscillation patterns in the future will probably cause a return to declining wind speeds. Anticipating these changes is important for the wind power industry. Wind farms should be constructed in areas with stable winds and high effective utilization hours (for example, 3–25 m s^{-1}). If high wind speeds are likely to be common, building turbines with larger capacities could be justified. For example, capturing more available wind energy (blue bars in Fig. 4d) could be achieved through the installation of higher capacity wind turbines (for example, General Electric GE 2.5-120, green bars in Fig. 4d), greatly increasing total power generation. Most turbines tend to require replacement after 12–15 years[41]. Further refinement of the relationships uncovered in this paper could allow choices of turbine capacity, rotor and tower that are optimized not just to wind speeds of the recent past but also to possible future changes during the lifespan of the turbines.

In summary, we find that after several decades of global terrestrial stilling, wind speed has rebounded, increasing rapidly across the globe in the decade since 2010. Ocean–atmosphere oscillations, rather than increased surface roughness, are probably the causes. These findings are important for those vested in maximizing the potential of wind as an alternative energy source. The development

of renewable energy sources, including wind power[6–9,40], is central to energy scenarios[8] that help keep warming below 2 °C. One megawatt of wind power reduces 1,309 tonnes of carbon dioxide emissions and also saves 2,000 litres of water compared with other energy sources[9,40]. Since its debut in the 1980s, the total global wind power capacity reached 539 gigawatts by the end of 2017, and the wind power industry is still booming globally. For instance, the total wind power capacity in the United States alone is projected to increase fourfold by 2050 (ref. [9]). The reversal in global terrestrial stilling bodes well for the expansion of large-scale and efficient wind power generation systems in these mid-latitude countries in the near future.

Online content

Any methods, additional references, Nature Research reporting summaries, source data, extended data, supplementary information, acknowledgements, peer review information; details of author contributions and competing interests; and statements of data and code availability are available at https://doi.org/10.1038/s41558-019-0622-6.

References

1. Roderick, M. L., Rotstayn, L. D., Farquhar, G. D. & Hobbins, M. T. On the attribution of changing pan evaporation. *Geophys. Res. Lett.* **34**, 1–6 (2007).
2. Vautard, R., Cattiaux, J., Yiou, P., Thépaut, J. N. & Ciais, P. Northern Hemisphere atmospheric stilling partly attributed to an increase in surface roughness. *Nat. Geosci.* **3**, 756–761 (2010).
3. Mcvicar, T. R., Roderick, M. L., Donohue, R. J. & van Niel, T. G. Less bluster ahead? Ecohydrological implications of global trends of terrestrial near-surface wind speeds. *Ecohydrology* **5**, 381–388 (2012).
4. McVicar, T. R. et al. Global review and synthesis of trends in observed terrestrial near-surface wind speeds: implications for evaporation. *J. Hydrol.* **416–417**, 182–205 (2012).
5. Tian, Q., Huang, G., Hu, K. & Niyogi, D. Observed and global climate model based changes in wind power potential over the northern hemisphere during 1979–2016. *Energy* **167**, 1224–1235 (2019).
6. Lu, X., McElroy, M. B. & Kiviluoma, J. Global potential for wind-generated electricity. *Proc. Natl Acad. Sci. USA* **106**, 10933–10938 (2009).
7. *Adoption of the Paris Agreement* FCCC/CP/2015/L.9/Rev.1 (UNFCCC, 2015).
8. IPCC *Climate Change 2014: Mitigation of Climate Change* (eds Edenhofer, O. et al.) (Cambridge Univ. Press, 2014).
9. *Projected Growth Wind Industry Now until 2050* (US Department of Energy, 2018).
10. Nathan, R. & Muller-landau, H. C. Spatial patterns of seed dispersal, their determinants and consequences for recruitment. *Trends Ecol. Evol.* **15**, 278–285 (2000).
11. Torralba, V., Doblas-Reyes, F. J. & Gonzalez-Reviriego, N. Uncertainty in recent near-surface wind speed trends: a global reanalysis intercomparison. *Environ. Res. Lett.* **12**, 114019 (2017).
12. Wu, J., Zha, J. L., Zhao, D. M. & Yang, Q. D. Changes in terrestrial near-surface wind speed and their possible causes: an overview. *Clim. Dynam.* **51**, 2039–2078 (2018).
13. Nchaba, T., Mpholo, M. & Lennard, C. Long-term austral summer wind speed trends over southern Africa. *Int. J. Climatol.* **37**, 2850–2862 (2017).
14. Chen, L., Li, D. & Pryor, S. C. Wind speed trends over china: quantifying the magnitude and assessing causality. *Int. J. Climatol.* **33**, 2579–2590 (2013).
15. Naizghi, M. S. & Ouarda, T. B. Teleconnections and analysis of long-term wind speed variability in the UAE. *Int. J. Climatol.* **37**, 230–248 (2017).
16. Guo, H., Xu, M. & Hu, Q. Changes in near-surface wind speed in China: 1969-2005. *Int. J. Climatol.* **31**, 349–358 (2011).
17. Wu, J., Zha, J. L., Zhao, D. M. & Yang, Q. D. Changes of wind speed at different heights over eastern China during 1980–2011. *Int. J. Climatol.* **38**, 4476–4495 (2018).
18. Zhu, Z. et al. Greening of the Earth and its drivers. *Nat. Clim. Change* **6**, 791–796 (2016).
19. Kim, J. C. & Paik, K. Recent recovery of surface wind speed after decadal decrease: a focus on South Korea. *Clim. Dynam.* **45**, 1699–1712 (2015).
20. Azorin-Molina, C. et al. Homogenization and assessment of observed near-surface wind speed trends over Spain and Portugal, 1961–2011. *J. Clim.* **27**, 3692–3712 (2014).
21. Tobin, I., Berrisford, P., Dunn, R. J. H., Vautard, R. & McVicar, T. R. in *State of the Climate in 2013* (eds Blunden, J. & Arndt, D. T.) S28–S29 (American Meteorological Society, 2014).
22. Toms, J. D. & Lesperance, M. L. Piecewise regression: a tool for identifying ecological thresholds. *Ecology* **84**, 2034–2041 (2003).
23. Ryan, S. E. & Porth, L. S. *A Tutorial on the Piecewise Regression Approach Applied to Bedload Transport Data* (CreateSpace Independent Publishing Platform, 2015).
24. Dunn, R. J. H., Willett, K. M., Morice, C. P. & Parker, D. E. Pairwise homogeneity assessment of HadISD. *Clim. Past* **10**, 1501–1522 (2014).
25. Pettitt, A. N. A non-parametric approach to the change-point problem. *J. R. Stat. Soc. Ser. C* **28**, 126–135 (1979).
26. Zeng, Z. et al. Global terrestrial stilling: does Earth's greening play a role? *Environ. Res. Lett.* **13**, 124013 (2018).
27. Draper, N. R. & Smith, H. *Applied Regression Analysis* 3rd edn (Wiley-Interscience, 1998).
28. Wang, C. Z. Atlantic climate variability and its associated atmospheric circulation cells. *J. Clim.* **15**, 1516–1536 (2002).
29. Hurrell, J. W., Kushnir, Y., Ottersen, G. & Visbeck, M. (eds) *The North Atlantic Oscillation Climatic Significance and Environmental Impact* (American Geophysical Union, 2003).
30. Zhang, Y., Xie, S.-P., Kosaka, Y. & Yang, J.-C. Pacific decadal oscillation: tropical Pacific forcing versus internal variability. *J. Clim.* **31**, 8265–8279 (2018).
31. Timmermann, A. et al. El Niño-southern oscillation complexity. *Nature* **559**, 535–545 (2018).
32. Dee, D. P. et al. The ERA–Interim reanalysis: configuration and performance of the data assimilation system. *Q. J. R. Meteorol. Soc.* **137**, 553–597 (2011).
33. Pryor, S. C. et al. Wind speed trends over the contiguous US. *J. Geophys. Res. D* **114**, D14105 (2009).
34. Wind-turbine-models.com. *General Electric GE 2.5-120* https://www.en.wind-turbine-models.com/turbines/310-general-electric-ge-2.5-120 (2018).
35. Steinman, B. A. et al. Atlantic and Pacific multidecadal oscillations and northern hemisphere temperatures. *Science* **347**, 988–991 (2015).
36. Tobin, I. et al. Climate change impacts on the power generation potential of European mid-century wind farms scenario. *Environ. Res. Lett.* **11**, 034013 (2016).
37. US Energy Information Administration. *Capacity Factors for Utility Scale Generators Not Primarily Using Fossil Fuels, January 2013–July 2019* https://www.eia.gov/electricity/monthly/epm_table_grapher.php?t=epmt_6_07_b (2018).
38. Dell, J. & Klippenstein, M. *Wind Power Could Blow Past Hydro's Capacity Factor by 2020* https://www.greentechmedia.com/articles/read/wind-power-could-blow-past-hydros-capacity-factor-by-2020 (2018).
39. Wind-turbine-models.com. *General Electric GE 1.85-87* https://www.en.wind-turbine-models.com/turbines/745-general-electric-ge-1.85-87 (2018).
40. *Global Wind Report 2018* (Global Wind Energy Council, 2019).
41. Hughes, G. *The Performance of Wind Farms in the United Kingdom and Denmark* (Renewable Energy Foundation, 2012).
42. Morice, C. P., Kennedy, J. J., Rayner, N. A. & Jones, P. D. Quantifying uncertainties in global and regional temperature change using an ensemble of observational estimates: the HadCRUT4 data set. *J. Geophys. Res. Atmos.* **117**, 1–22 (2012).
43. Reynolds, R. W., Rayner, N. A., Smith, T. M., Stokes, D. C. & Wang, W. An improved in situ and satellite SST analysis for climate. *J. Clim.* **15**, 1609–1625 (2002).

Methods

Wind datasets. The key data used in this analysis is the Global Surface Summary of the Day (GSOD) database processed by the US National Climatic Data Center (downloaded 1 August 2018 from ftp://ftp.ncdc.noaa.gov/pub/data/gsod). The database is derived from the United States Air Force DATSAV3 surface data and the Federal Climate Complex Integrated Surface Hourly dataset based on data exchanged through the World Meteorological Organization (WMO) World Weather Watch Programme according to WMO Resolution 40 (Cg-XII)[44]. There is a total of 28,149 stations included in the GSOD database globally (for distributions see the dots in Supplementary Fig. 3). The original records from all the weather stations have undergone extensive quality control procedures (more than 400 algorithms, see www.ncdc.noaa.gov/isd for details). These synoptic hourly observations were processed into mean daily values from recorded hourly data by the National Climatic Data Center.

We focus our study on the decadal variation of wind speed and other wind variables (maximum sustained wind speed, maximum wind gust) for the 40-yr period of 1978–2017, when the data are the most complete. When selecting the final subset of stations, we employ strict selection criteria to avoid including incomplete data series. First, we only select stations with complete data for all the 40 years of the analysis (1978–2017), with each year having complete records for all 12 months. Second, each monthly value has to be derived from at least 15 d of data. The daily values have to be derived from a minimum of four observations. As a result, only 1,435 stations are included for analysis (locations are shown in Supplementary Fig. 3; the mean number of observations in a day is shown in Supplementary Fig. 10; code and processed data are available in Supplementary Data 1). Among them, 543 stations are automatic monitoring stations that are in operation during the entire study period. For some analyses (Supplementary Fig. 7) we relax our selection criteria to include more stations, for instance by allowing 1, 5, 10 or 20 years of missing data. Last, the results show no dependence on whether global mean annual wind speed or global median annual wind speed is used to describe the decadal variation of global wind speed (Supplementary Fig. 21 versus Fig. 1a).

We also repeat the wind analyses using the HadISD (v.2.0.2.2017f)[24] global subdaily database, which is distributed by the UK Met Office Hadley Centre and is freely accessed from https://www.metoffice.gov.uk/hadobs/hadisd/. The total number of stations in HadISD is 8,103, all of which passed quality control tests that are designed to remove bad data while also keeping the extremes of wind speed and direction, temperature, dew point temperature, sea-level pressure and cloud data (total, low, mid and high level). For example, a set of quality control procedures[24] (such as duplicate check, distributional gap check, neighbour outlier check and so on) has been performed on the major climatological variables. In our analysis, we use the criteria that are described above to select stations that have uninterrupted, continuous monthly records during the period 1978–2017 ($n = 1,542$; code and processed data are available in Supplementary Data 2).

Climate indices. The dynamics of ocean–atmospheric circulations can be described with climate indices. Almost all climate indices are associated, to some extent, with regional surface temperature anomalies (or temperature heterogeneity), in particular SST. We select 21 time series of climate indices describing monthly atmospheric and oceanic phenomena to compare decadal variations of the Earth's climate system with changes in wind speed (Supplementary Table 2). Only indices that are available for the whole study period (1978–2017) are considered (downloaded from https://www.esrl.noaa.gov/psd/data/climateindices/list/). For example, we include the following eight teleconnection indices: PDO; Pacific North American Index; Western Pacific Index; NAO; East Pacific/North Pacific Oscillation; North Pacific pattern; East Atlantic pattern and Scandinavia pattern. We also include one atmospheric index (Arctic Oscillation) and one multivariate El Niño–Southern Oscillation index. We include six indices describing regional SST in Pacific oceans: Eastern Tropical Pacific SST (5° N–5° S, 150° W–90° W) (NINO3); Central Tropical Pacific SST (5° N–5° S, 160° E–150° W) (NINO4); Extreme Eastern Tropical Pacific SST (0–10° S, 90° W–80° W) (NINO12); East Central Tropical Pacific SST (5° N–5° S, 170° W–120° W) (NINO34); Oceanic Nino Index; and Western Hemisphere Warm Pool. Two of the indices describe regional SST in Atlantic oceans: TNA and the Tropical Southern Atlantic Index. The final three indices are the Atlantic Meridional Mode, the Southern Oscillation Index and the 10.7-cm Solar Flux (Solar). All these indices are widely used by the climate community and are informative regarding the decadal variations of ocean–atmospheric circulations.

Statistical analyses. It is apparent that the trend varies in the time series of global and/or regional-average mean annual wind speed for different ranges of year (for example, Fig. 1a). A traditional single linear model does not provide an adequate description of a change in the tendency and, therefore, we apply a piecewise linear regression model[22,23] to quantify potential turning points in a given time series. Piecewise linear regression is capable of detecting where the slope of a linear function changes and allows multiple linear models to be fitted to each distinct section of the time series. For a time series y (for example, global average mean annual wind speed), a continuous piecewise linear regression model with one turning point (TP) can be described as:

$$y = \begin{cases} \beta_0 + \beta_1 t + \varepsilon, & t \leq \text{TP} \\ \beta_0 + \beta_1 t + \beta_2 (t - \text{TP}) + \varepsilon, & t > \text{TP} \end{cases} \quad (3)$$

where t is year, β_0, β_1 and β_2 are regression coefficients and ε is the residual of the regression. The linear trend is β_1 before the TP (year) and $\beta_1 + \beta_2$ after the TP. We use least-squares error techniques to fit the model to the data and determine TP, β_0, β_1 and β_2. To avoid linear regression in a period with too few years, we confine TP to be within the period of 1980–2015. The necessity of introducing TP is tested statistically with the t-test under the null hypothesis that 'β_2 is not different from zero'. The diagnostic statistics for the regression also include the goodness-of-fit (R^2), the P value for the whole model and the P values for the trends before and after TP. We consider $P < 0.05$ as significant.

In addition, we use a forward stepwise regression algorithm[27] to select major climate indices that have the largest explanatory power for the decadal variations in wind speed. The algorithm is a systematic method for adding predictors from a multilinear model according to their statistical significance in explaining the response (decadal variation of u in this study). The initial regression model contains only an intercept term. The explanatory power of incrementally larger and smaller models is then compared to determine which predictor should be included. At each step, the P value of an F statistic is calculated to examine models with a potential predictor that is not already in the model. The null hypothesis is that the predictor has a zero coefficient if included in the model. If there is sufficient evidence at a given significant level to reject the null hypothesis, the predictor is added to the model. Therefore, the earlier the predictor enters the model, the larger the explanatory power the predictor has.

We apply the forward stepwise regression to determine six climate indices (referred to as major indices hereafter) from a generalized linear model according to their statistical significance in explaining wind speed. We use only six indices in the regression because the fit improvement becomes marginal when the number of indices retained in the stepwise regression is greater. The regression model is then applied to reconstruct interannual variations of wind speed over the globe and/or the regions using the selected six climate indices. The forward stepwise regression is first applied to the original time series considering the total variances, and then applied to the detrended time series to exclude the variances from linear trends (Supplementary Figs. 15 and 16). Last, to test whether these climate indices can be used to predict wind speed, we further train the models using only the detrended time series before the turning points. We then compare the reconstructed wind speed with the observed wind speed after the turning points (Fig. 2).

Analyses on the possible causes for the interannual variability of wind speed. The indicators (climate indices) significantly correlated with wind speed on a global scale include TNA ($R = -0.50$, $P < 0.01$), PDO ($R = 0.46$, $P < 0.01$), Western Hemisphere Warm Pool ($R = -0.46$, $P < 0.01$), NAO ($R = 0.39$, $P < 0.05$), Atlantic Meridional Mode ($R = -0.39$, $P < 0.05$), East Pacific/North Pacific Oscillation ($R = 0.37$, $P < 0.05$), Tropical Southern Atlantic Index ($R = -0.38$, $P < 0.05$), Solar ($R = 0.35$, $P < 0.05$), Southern Oscillation Index ($R = -0.32$, $P < 0.05$) and East Atlantic pattern ($R = 0.31$, $P < 0.05$). Overall, the 21 climate indices explain 90% of the interannual variation in global mean annual wind speed (adjusted $R^2 = 78\%$). Regionally, they explain 91%, 75% and 87% of the interannual variation in mean annual wind speed for North America (adjusted $R^2 = 81\%$), Europe (adjusted $R^2 = 46\%$) and Asia (adjusted $R^2 = 71\%$), respectively.

To avoid overfitting, we use stepwise linear regression to discuss whether multiple regression of six indices can reconstruct interannual variations of wind speed over the globe and/or regions. To estimate the uncertainty associated with samples, we randomly select 40% of stations for the calculation of global/regional wind speed and repeat the analyses 300 times. The number in parentheses in Supplementary Table 3 shows how many times climate indices are selected as six major predictors. These climate indices explain $70 \pm 5\%$, $79 \pm 3\%$, $48 \pm 9\%$ and $51 \pm 8\%$ of the interannual variation in mean annual wind speed for the globe, North America, Europe and Asia, respectively (Supplementary Table 3 and Fig. 15). Furthermore, we also test stepwise regression analysis after detrending all data, although this adjustment may mask relationships underlying long-term stilling. The goodness-of-fit decreased as expected when the stilling trend is removed (Supplementary Fig. 16). However, detrended indices still significantly explain detrended variation of wind speed, particularly the recent reversal (Supplementary Fig. 16), which supports the robustness of the regression analyses.

The greatest explanatory power factor for each region is associated with the following indices: TNA for North America ($R = -0.67$, $P < 0.001$); NAO for Europe ($R = 0.37$, $P < 0.05$) and PDO for Asia ($R = 0.50$, $P < 0.01$) (Supplementary Tables 2 and 3). These three indices are also significantly correlated with global mean annual wind speed ($P < 0.01$; Supplementary Table 2). We further conduct Granger causality tests[45] in which we select lag length using a Bayesian information criterion. Global mean annual wind speed is 'Granger-caused' by TNA ($P < 0.001$), NAO ($P < 0.01$) and PDO ($P < 0.1$). Regionally, the tests also reject the null hypothesis that (1) TNA does not Granger-cause wind speed over North America ($P < 0.001$), (2) NAO does not Granger-cause wind speed over Europe ($P < 0.1$) and (3) PDO does not Granger-cause wind speed over Asia ($P = 0.11$). In addition, although the reversal of winds and the retained climate indices differ in regions, owing to ocean–atmosphere oscillations having some degree of synchronization

during turning points of multidecadal climate variability[46], the pattern of terrestrial stilling and its reversal seems to be synchronized.

PDO and TNA are important predictors regardless of the subset of stations used; however, although NAO has the largest explanatory power for regional wind speed over Europe, there are 169/300 cases in which NAO is not included as a major predictor (Supplementary Table 3). Thus, even within Europe, the impact of NAO differs regionally. We therefore investigate the spatial patterns of the correlation between the three indices (PDO, TNA, NAO) and the regional winds (Fig. 3c–e). The regional wind is calculated using all stations within a 5° × 5° cell; and only the cells with more than three stations are included in the analysis. TNA has a strong significant negative correlation with regional wind speed in North America, excluding western Canada and areas near Mexico (Fig. 3c). PDO has a significant positive correlation with regional wind speed globally (Fig. 3e). NAO has an overwhelmingly significant positive correlation with regional wind speed in the United States and Northern Europe, in particular the United Kingdom. In contrast, it has a negative correlation with regional wind speed in southern Europe (Fig. 3d). Statistically, NAO is negatively correlated with European winds south of 48° N ($R = -0.39$, $P < 0.05$), whilst it is significantly and positively correlated with European winds north of 48° N ($R = 0.48$, $P < 0.01$).

Calculations for wind power assessments. Due to the nonlinear relationship between wind power and wind speed (equation (1)), high temporal resolution data are needed for wind speed to produce an accurate estimate of wind power. Thus, we use the HadISD global subdaily database from the UK Met Office Hadley Centre[24]. For each station that has uninterrupted continuous monthly records during the period 1978–2017 ($n = 1,542$), we use linear interpolation to interpolate a subdaily time series to an hourly time series. Figure 4a shows the frequency distributions of global average hourly wind speed in 2010 and 2017, and also for the year 2024, assuming the same increasing rate.

We then discuss annual wind power production given these hourly wind speed time series for 2010, 2017 and 2024, considering that production is dependent on the specifications of wind turbines. Here we use General Electric GE 2.5-120 (ref. [34]) as an example. The parameters for this turbine include the following: rated power, 2,500.0 kW; cut-in wind speed, 3.0 m s^{-1}; cut-out wind speed, 25.0 m s^{-1}; diameter, 120 m; swept area, 11,309.7 m^2 and hub height: 110/139 m (here we take 120 m). The power curve for this turbine is shown in Supplementary Fig. 22. The wind speed time series (2010, 2017 and 2024) at the height of the turbine (that is, 120 m) is first estimated using the wind profile power law (equation (2)), and then converted into the hourly wind power (Supplementary Fig. 19) using the power curve (Supplementary Fig. 22). Due to the increased frequency of high wind speed, annual wind power production from the turbine increases from 2.4×10^6 kWh in 2010 to 2.8×10^6 kWh in 2017, and then to 3.3×10^6 kWh in 2024. As a result, the overall capacity factor increases 1.9% during 2010–2017 and 2.2% during 2018–2024.

To compare the significance of the increased capacity factor induced by the strengthening wind speed with that due to technology innovation (for example, improvement of the turbine's power efficiency), we collect the overall capacity factor for wind generation in the United States from the US Energy Information Administration[37] (black line in Fig. 4b). In the United States, the overall capacity factor is highly correlated with the cube of the regional-average wind speed (u^3) ($R = 0.86$, $P < 0.01$; Fig. 4b). Even for the detrended time series, the correlation coefficient between the capacity factor and the cube of the regional-average wind speed is as high as 0.71 ($P < 0.05$), showing that wind speed is a key factor for the year-to-year variation of wind power energy production. It is well known that technology innovation is a key factor that drives the increase of capacity factor for wind generation[38]. To isolate the wind speed-induced increase in capacity factor from that due to technology innovation, we use the regional mean hourly wind speed in 2010, 2017 and 2024 (assuming the same increasing rate) to estimate the increase of capacity factor for a given turbine, thereby controlling for technology innovation. The wind speed-induced increase in capacity factor is +2.5% between 2010 and 2017 and +3.2% between 2017 and 2024. This explains more than 50% of the overall increase of capacity factor for wind generation in the United States.

We also collect information regarding the installed turbines from the US Wind Turbine Database ($n = 57,646$; https://eerscmap.usgs.gov/uswtdb) (for locations refer to Supplementary Fig. 23). The turbine that was nearest to one of the HadISD weather stations ($n = 1,542$) is at Deaf Smith County in the United States (<1 km; wind farm name: Hereford 1; case ID: 3047384; location see the inset plot in Fig. 4c). The turbine was installed in 2014. The turbine is a General Electric GE 1.85-87 (ref. [39]). The parameters for this turbine include: rated power, 1,850.0 kW; cut-in wind speed, 3.0 m s^{-1}; rated wind speed, 12.5 m s^{-1}; cut-out wind speed, 25.0 m s^{-1}; diameter, 87.0 m; swept area, 5,945.0 m^2 and hub height: 80 m. We combine these parameters with equation (1) to estimate the power curve for the turbine (Supplementary Fig. 24). Finally, we integrate the power curve with the hourly wind speed from 1978 to 2017 at the hub height at this station to calculate annual wind power production generated by the General Electric GE 1.85-87 turbine (Supplementary Fig. 25a; red bars in Fig. 4d). In addition, we calculate annual wind power production at the station generated by the General Electric GE 2.5-120 turbine (Supplementary Fig. 25b; green bars in Fig. 4d). We also use equation (1) to estimate maximum annual wind power production at the station using a

diameter of 120 m and hub height of 120 m (the same as the General Electric GE 2.5-120 turbine), which is constrained by the Betz limit ($f = 16/27$ in equation (1)) (Supplementary Fig. 25c; blue bars in Fig. 4d). The Betz limit describes the theoretical maximum ratio of power that can be extracted by a wind turbine to the total power contained in the wind. We used three reanalysis datasets[47–49] and the satellite-observed changes of vegetation activity[50] and urban extent[51] over land for the past decades.

Reporting Summary. Further information on research design is available in the Nature Research Reporting Summary linked to this article.

Data availability

Code availability

References

44. *WMO Resolution 40 (Cg-XII). WMO Policy and Practice for the Exchange of Meteorological and Related Data and Products including Guidelines on Relationships in Commercial Meteorological Activities* (World Meteorological Organisation, 1996).
45. Granger, C. W. J. Investigating causal relations by econometric models and cross-spectral methods. *Econometrica* **37**, 424–438 (1969).
46. Henriksson, S. V. Interannual oscillations and sudden shifts in observed and modeled climate. *Atmos. Sci. Lett.* **19**, e850 (2018).
47. *NCEP/NCAR Global Reanalysis Products, 1948–continuing* (NCAR/UCAR Research Data Archive, accessed 10 August 2018); http://rda.ucar.edu/datasets/ds090.0/
48. *ERA-Interim Project* (NCAR/UCAR Research Data Archive, accessed 10 August 2018); https://doi.org/10.5065/D6CR5RD9
49. *ERA5: Fifth Generation of ECMWF Atmospheric Reanalyses of the Global Climate* (Copernicus Climate Data Store, accessed 25 May 2019); https://cds.climate.copernicus.eu/cdsapp#!/home
50. Zhu, Z. et al. Global data sets of vegetation leaf area index (LAI)3g and fraction of photosynthetically active radiation (FPAR)3g derived from global inventory modeling and mapping studies (GIMMS) normalized difference vegetation index (NDVI3G) for the period 1981 to 2011. *Remote Sens.* **5**, 927–948 (2013).
51. Liu, X. et al. High-resolution multi-temporal mapping of global urban land using landsat images based on the Google Earth engine platform. *Remote Sens. Environ.* **209**, 227–239 (2018).

Acknowledgements

Author contributions

Z.Z. and E.F.W. designed the research. Z.Z. and L.Y. performed the analysis. Z.Z., A.D.Z. and T.S. wrote the draft. All authors contributed to the interpretation of the results and the writing of the paper.

Competing interests

The authors declare no competing interests.

Additional information

Supplementary information is available for this paper at https://doi.org/10.1038/s41558-019-0622-6.

Correspondence and requests for materials should be addressed to Z.Z.

Peer review information *Nature Climate Change* thanks Sonia Jerez and the other, anonymous, reviewer(s) for their contribution to the peer review of this work.

Reprints and permissions information is available at www.nature.com/reprints.